Simultaneous Identification and Control Using Active Signal Injection for Series Hybrid Electric Vehicles Based on Dynamic Programming

Haojie Zhu, *Student Member, IEEE*, Ziyou Song, *Member, IEEE*, Jun Hou, *Member, IEEE*, Heath F. Hofmann, *Senior Member, IEEE*, and Jing Sun, *Fellow, IEEE*

***Abstract*— Hybrid electric vehicles (HEVs) are overactuated systems in that they include two power sources: a battery pack and an internal combustion engine. This feature of HEVs is exploited in this article to achieve accurate identification of battery parameters/states. By actively injecting currents, the state of charge, state of health, and other battery parameters can be estimated in a specific sequence to improve identification performance when compared to the case where all parameters and states are estimated concurrently using baseline currents. A dynamic programming strategy is developed to provide the benchmark results regarding how to balance the conflicting objectives corresponding to the identification and system efficiency. The tradeoff between different objectives is presented to optimize the current profile so that the richness of the signal can be ensured and the good fuel economy can be achieved. In addition, simulation results show that the root-mean-square error of the estimation can be decreased by up to 100% at a cost of less than a 2% increase in fuel consumption. With the proposed simultaneous identification and control algorithm, the parameters/states of the battery can be monitored to ensure safe and efficient operation of the battery for HEVs.**

***Index Terms*— Dynamic programming, fuel economy, hybrid electric vehicle (HEV), lithium-ion battery, simultaneous identification and control, state of charge (SOC)/state of health (SOH) identification.**

I. Introduction

THE pursuit to improve the efficiency and diminish the pollution emissions of vehicles has resulted in the development of hybrid electric vehicles (HEVs) [1]–[3]. Compared with conventional vehicles, HEVs adopt an extra power source (i.e., batteries) as a buffer to increase overall engine efficiency [4]. Accurate parameter and state identification of batteries, including state of health (SOH) and state of charge (SOC), is fundamental for the efficient and safe operation of HEVs [5], [6]. Condition monitoring of the battery is crucial, as effective monitoring can help avoid violating the operating constraints (e.g., overcharge/overdischarge) and therefore prolong the battery life [7]. However, parameter estimation and fuel consumption optimization generally conflict because the power management strategy (PMS) that minimizes the fuel consumption does not necessarily ensure a battery current profile, which contains sufficiently rich information for estimation. Single power source systems cannot achieve these two objectives concurrently. However, for an overactuated system (e.g., HEVs), the extra degree of freedom in power allocation can be used to achieve simultaneous identification and control (SIC) [8]. There exists related work which achieves parameters estimation and output regulation at the same time in overactuated systems. For instance, Hasanzadeh *et al.* [9] focused on induction machines and achieved the identification of rotor resistance and minimization of the torque ripple through the injection of a relatively low-frequency signal. Reed *et al.* [10] also studied the overactuated features of permanent magnet synchronous machines in order to simultaneously estimate parameters and regulate torque. Leve *et al.* [11] injected signals in order to estimate parameters without disturbing the control objectives after exploiting the "null motio" of overactuated spacecraft. Similarly, Chen and Wang [12] exploited multiple motors in a vehicle to inject additional excitation so that the tire-road friction coefficient can be identified accurately, given the extra degrees of freedom provided by electric vehicles. In addition, Song *et al.* [13] optimized the current profile of the battery adopted in the battery/supercapacitor hybrid energy storage system using model predictive control in order to achieve SIC. This article proposes SIC for HEVs to significantly improve the estimation performance of battery parameters/states with a slight increase in fuel consumption.

Most HEVs can be classified into three categories: 1) series [14]; 2) parallel [15]; 3) power split [16]. In this article, the series HEV is studied because the internal combustion engine (ICE) is mechanically decoupled from the wheels [17], which means that the working point of the ICE determined by the speed and torque can always be optimal. Since HEVs are sophisticated electromechanical-chemical systems, a PMS is required to fulfill the control objectives, including increasing the system efficiency and reducing pollution emissions [18]. In the existing literature, many PMSs have been designed, which can be categorized into rule-based control

Manuscript received October 17, 2019; revised December 20, 2019; accepted January 21, 2020. Date of publication January 27, 2020; date of current version March 20, 2020. *(Corresponding authors: Ziyou Song; Jun Hou.)*

Haojie Zhu is with the Department of Mechanical Engineering, University of Michigan, Ann Arbor, MI 48105 USA (e-mail: zhuhj@umich.edu).

Ziyou Song and Jing Sun are with the Department of Naval Architecture and Marine Engineering, University of Michigan, Ann Arbor, MI 48105 USA (e-mail: ziyou@umich.edu; jingsun@umich.edu).

Jun Hou and Heath F. Hofmann are with the Department of Electrical Engineering and Computer Science, University of Michigan, Ann Arbor, MI 48105 USA (e-mail: junhou@umich.edu; hofmann@umich.edu).

Digital Object Identifier 10.1109/TTE.2020.2969811

and optimization-based control [19]. More and more attention is being paid to optimization-based control, which can be classified into two types [20]: 1) global optimization, such as dynamic programming (DP) [21] and 2) real-time optimization [22]. Among most of the PMSs for HEVs, constant battery parameters are assumed, meaning that they neglect the variation of parameters due to battery degradation and varying operating conditions. This assumption could result in unsafe and inefficient operation of HEVs because cell impedance increase caused by battery degradation will raise the possibility of overcharge and/or overdischarge [23]. This specific concern motivates us to apply SIC to HEVs.

To identify the battery's states and parameters, an estimation approach based on the equivalent circuit model (ECM) [24] is used for its simplicity and adequate accuracy [25]. SOC estimation approaches include Coulomb counting, extended Kalman filter (EKF) [26], sliding mode observer [27], and recursive total least squares-based observer [28]. SOH, which represents the battery condition, is defined as the ratio of the remaining battery capacity to its original value [29]. It can be estimated through EKF [30], least-squares methods [31], and Lyapunov-based methods [32]. Since battery parameters need to be identified offline when adopting the estimation approaches mentioned earlier, parameter variations due to aging and changes in operating conditions (e.g., temperatures) can cause performance degradation [33]. To address this issue, a dual EKF (DEKF) is developed to identify SOH, SOC, and battery parameters (e.g., ohmic resistance) concurrently [34]. Besides the estimation algorithms, battery current and voltage, applied in the identification process as the input and output, can dramatically influence the estimation accuracy. Therefore, it is necessary to optimize the current waveform in order to ensure signal richness and therefore identification accuracy [35], [36].

Given the extra degree of freedom in PMSs offered by HEVs, it is possible to inject sufficiently rich signals and satisfy operating requirements simultaneously. In order to optimize the performance of SIC, an innovative DP-based method is adopted in this article. The sequential algorithm, which separates signals according to frequency and identifies parameters/states in a specific sequence through active current injection, is proven to be more effective than DEKF, which concurrently identifies all the parameters and states according to the experimental results [37]. This article integrates the sequential algorithm in the DP framework to improve the estimation performance. The offline estimated battery parameters are used to determine the frequencies of the injected signals and provide the basic knowledge on ranges for different parameters/states. Thus, real-time monitoring of the battery states is achieved to prolong battery lifetime and improve efficiency. We believe that this is the first article exploiting the overactuated feature of HEVs to inject active signals into the battery for better estimation performance. Even though the signal injection induces a slight increase in fuel consumption, the accuracy of battery parameters/states estimation is significantly improved, which is important for the safe, efficient, and reliable application of lithium-ion batteries [38].

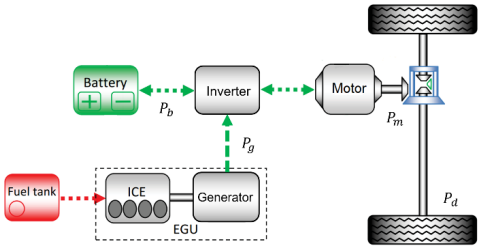

Fig. 1. Series HEV powertrain [39].

In summary, this article first investigates the overactuated feature of HEVs and combines fuel economy optimization with active battery monitoring. The energy management problem is solved using an innovative DP formulation. In order to optimize the profile of the injected current signal, the tradeoff between estimation accuracy and fuel consumption is also studied.

In this article, the series HEV model is presented and explored in Section II. The DP formulation is developed and presented in Section III along with a review of the sequential algorithm. Section IV discusses the simulation results of the proposed SIC and provides a comparison with the baseline results without active signal injection. Finally, Section V draws the conclusions.

II. Modeling of Series HEV

The series HEV, whose architecture is presented in Fig. 1, is studied in this article as an example; the SIC approach can work on all HEV topologies. The series powertrain is composed of an engine-generator unit (EGU), a battery, a motor, and an associated inverter. Since there are two power sources (i.e., EGU and battery), which provide the overactuated feature, the model fulfills the following energy balance equations:

$$P_d(t) = P_m(t) \tag{1}$$

$$P_m(t) = \eta_m(t)[P_g(t) + P_b(t)] \tag{2}$$

where $P_d(t)$, obtained from (3)–(5), is defined as the demand power for the vehicle to follow the driving cycle, $P_m(t)$ is defined as the motor power, $\eta_m(t)$, shown in Fig. 2, is defined as the efficiency of the combination of motor and inverter, which is related to motor speed and torque, $P_g(t)$ is the generator power, and $P_b(t)$ is the battery power. Since the generator has high efficiency over a wide operating range, the generator is assumed to have the constant efficiency, e.g., 95%, in order to simplify the analysis.

A. Vehicle Model

The main parameters of the studied automobile model are listed in Table I and the basic dynamics are given as

$$v = \omega_m \times N_r \times R_w. \tag{3}$$

1) *Regenerative Braking Mode:*

$$P_d/\eta_r - (\mathrm{mgfv}\cos\theta + \mathrm{mgv}\sin\theta + 0.5C_D\rho A_f v^3) = \mathrm{mv}\dot{v}. \tag{4}$$

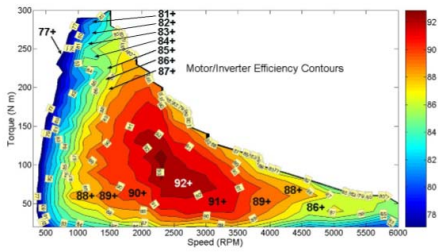

Fig. 2. Motor/inverter efficiency contours [40].

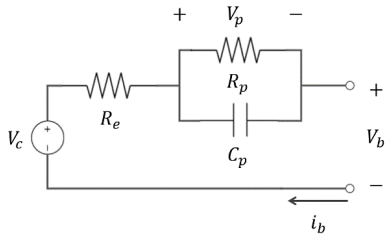

Fig. 3. First-order ECM.

TABLE I
BASIC PARAMETERS OF THE SERIES HEV MODEL [41]

Parameters	Values (Unit)
Vehicle Mass (m)	1254 kg
Wheel Radius (R_w)	0.287 m
Frontal Area of the Vehicle (A_f)	2.52 m^2
Air Drag Coefficient (C_D)	0.3
Rolling Resistance Coefficient (f)	0.015
Transmission Efficiency (η_T)	0.9
Regenerative Braking System Efficiency (η_r)	0.25
Final Transmission Ratio (N_r)	4.113
Nominal Voltage of Battery (V_0)	201.6V
Capacity of Battery Pack (Q_p)	6.5Ah
Ohmic Resistance of Battery Pack (R_b)	≈0.5Ω

2) *Traction Mode:*

$$P_d\eta_T-(\mathrm{mgfv}\cos\theta+\mathrm{mgv}\sin\theta+0.5C_D\rho A_f v^3)=\mathrm{mv}\dot{v} \tag{5}$$

where v is the automobile speed, ω_m is the motor speed, g is the gravitational acceleration, θ is the climbing angle, and ρ is the density of air.

B. Battery Model

The battery behavior in the PMS is represented by the Rint model [41], as the battery resistance will dominate the power loss. The main parameters of the battery pack, which characterizes the Rint model, are summarized in Table I. The battery output power, i.e., P_b, can be formulated as (6) based on the Rint model

$$P_b = V_0 i_b - i_b^2 R_b \tag{6}$$

where i_b is defined as the battery current (positive i_b means that the battery pack is discharging, while negative i_b represents charging).

In the estimation process, the battery model applied is a first-order ECM, as shown in Fig. 3. In Fig. 3, V_b represents the battery voltage, V_p represents the RC pair voltage, and V_C is the open-circuit voltage (OCV). Although higher order models are more accurate than the first-order ECM when applied in estimation algorithms, model accuracy and computational cost are two conflicting objectives [42]. The computational cost of parameter identification for higher order models is much larger and the requirement of signal richness is higher as well. For instance, seven parameters have to be estimated for the second-order ECM; consequently, the current signal must have at least four sinusoidal components to satisfy the richness condition [43], which is not practical. Therefore, this article applies the first-order ECM considering both model accuracy and computational simplicity. The model has the following dynamics as shown in (7) and the basic model parameters of the applied Samsung 18650 Lithium battery cell, listed in Table II, are determined through the static capacity Hybrid pulse tests at 20 °C [42]:

TABLE II
MAIN PARAMETERS OF THE SAMSUNG 18650 LITHIUM BATTERY CELL

Parameters	Value (Unit)
Cell Capacity (Q_b)	2.47 Ah
Nominal Voltage	3.63 V
Ohmic Resistance of the Battery Cell (R_e)	100 mΩ
Coulomb Efficiency (η_c)	0.98
Resistance of RC Pair (R_p)	≈30 mΩ
Time Constant of RC Pair(τ_p)	≈15 s
Standard Deviation of Voltage Measurement Noise (σV)	20 mV

$$\begin{cases} V_b = V_C - R_e i_b - V_p \\ V_p = R_p(i_b - C_p \dot{V}_p). \end{cases} \tag{7}$$

The relationship between OCV and the normalized SOC is formulated as follows [44]:

$$V_C(z) = C_1 - C_2 z - \frac{C_3}{z} + C_4 \ln z + C_5 \ln(1-z) \tag{8}$$

where C_{1-5} are the five parameters of the function. The normalized SOC, i.e., z, can be obtained by the following:

$$z = z_0 - \int_{t_i}^{t} \frac{\eta_c}{Q_b} i_b(\tau) d\tau \tag{9}$$

where the initial value of SOC is defined as z_0. C_{1-5} are determined through experiments to be 2.6995, 0.0574, −1.3967, −0.5508, and −0.0377, respectively [44].

III. REVIEW OF SEQUENTIAL ALGORITHM

The identification of battery states and parameters is an important, though difficult, task. According to the Cramer–Rao bound analysis, the sequential algorithm is more accurate than

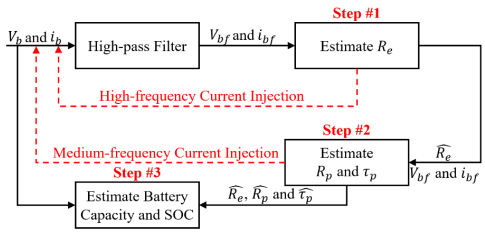

Fig. 4. Flowchart of sequential algorithm.

estimation algorithms that identify all the battery parameters and states concurrently [37]. This is because the sequential algorithm divides the estimation process into several steps. Therefore, a small number of battery parameters/states are identified in each step and fewer uncertainties are involved [37], [45], meaning that the estimation performance will be improved. To reduce the computational cost of estimation, (8) is linearized because the slope of OCV versus SOC curve does not change significantly within the normal operating range [42], [46]

$$V_C(z) = a_1\left(z_0 - \int_{t_i}^{t} \frac{\eta_c}{Q_b} i_b(\tau)d\tau\right) + a_2 \tag{10}$$

where a_1 and a_2 are two coefficients. After applying the Laplace transform, the battery dynamics in the frequency domain are obtained as follows:

$$V_b(s) = \frac{a_1 z_0 + a_2}{s} - \frac{a_1}{s}\frac{\eta_c}{Q_b} i_b(s) - R_e i_b(s) - \frac{R_p}{1+\tau_p s} i_b(s). \tag{11}$$

The Laplace transform of the battery terminal voltage is therefore composed of four parts, which are determined by the initial SOC, battery capacity, ohmic resistance, and parameters of the RC pair, respectively. Therefore, it is possible to separate the four components through filtering. The first term, related to the initial SOC, can be eliminated by a filter because it is constant in the time domain. The sequential algorithm can be summarized in three steps, as shown in Fig. 4 [37].

Step 1: After injecting the high-frequency current the resistance of the battery cell, which dominates the filtered battery voltage, i.e., $V_{\rm bf}$, is identified using EKF, which is one of the most common estimation algorithms. This identification approach can avoid the negative effects of process and measurement noise [47].

Step 2: Using the identified ohmic resistance, the parameters of the RC pair (i.e., the resistance R_p and the capacitance C_p) are estimated also using EKF when the high-pass filter is incorporated to filter the first component of $V_b(s)$ and the medium-frequency current is injected.

Step 3: Using all the identified parameters in Steps 1 and 2, the SOC and SOH are then identified based on the unfiltered signal simultaneously. Since DEKF is usually applied to estimate parameters and states concurrently [48], it is used in this step and it has the same state-space equation as EKF.

IV. Simultaneous Estimation and Optimization Using DP

The DP approach is applied to balance the parameter/state estimation and system optimization objectives as they are generally conflicting with each other. The baseline DP without active signal injection, denoted as DP−, is discussed first as follows:

$$J_{\rm DP-} = \sum_{j=1}^{T_f} \phi(P_g(j) \times T_s) + \gamma\, \Delta_{\rm SOC} \tag{12}$$

and

$$\Delta_{\rm SOC} = \begin{cases} 0, & \text{if } {\rm SOC}(T_f) \geq {\rm SOC}(1) \\ {\rm SOC}(T_f) - {\rm SOC}(1), & \text{otherwise} \end{cases}$$

subject to the constraints

$$\begin{aligned} {\rm SOC}_{\rm lb} \leq {\rm SOC}(j) &\leq {\rm SOC}_{\rm ub} \\ P_{b,\rm lb} \leq P_b(j) &\leq P_{b,\rm ub} \\ P_{g,\rm lb} \leq P_g(j) &\leq P_{g,\rm ub} \\ {\rm SOC}(T_f) &= {\rm SOC}(1) \\ P_g(j) + P_b(j) &= P_d(j)/\eta_m(j) \end{aligned}$$

where ϕ is the instantaneous fuel consumption function, which is shown in Fig. 5 [49], j represents the time index, T_s is the sampling time, T_f represents the time length, γ is the penalty factor, ${\rm SOC}_{\rm lb}$ and ${\rm SOC}_{\rm ub}$ are the lower and upper bounds of the recommended usage range, i.e., 0.2–0.9, $P_{b,\rm lb}$ and $P_{b,\rm ub}$ are the lower and upper bounds of the battery power, respectively, and $P_{g,\rm lb}$ and $P_{g,\rm ub}$ are the lower and upper bounds of the generator power, respectively. For series HEVs, the ICE is mechanically decoupled from the wheels, and thus, the operating point of ICE, which is defined by its torque and speed, can be set without the restriction from wheels. Aimed at maximizing the efficiency of ICE, its working point is assumed to follow the basic operating line [49], as shown in Fig. 5. The penalty factor γ is used to force the final SOC to be equal to the initial SOC. To ensure efficient operation of the battery for multiple driving cycles, the SOC in one driving cycle should be constrained within the recommended window of operation. In addition, the final SOC is set to be equal to the initial SOC because different terminal SOC values increase the complexity of results comparison. After acquiring the current signal of DP−, the battery parameters and states are concurrently identified using DEKF for comparison.

When the current signal is injected, the formula of battery power and the constraints of DP need to be changed. Since a sinusoidal battery current is injected for battery parameters/states identification, the formula of the total battery current can be represented

$$i_b(j) = I_{\rm ex}\cos(2\pi f_i T_s j) + i_c(k) \tag{13}$$

where $I_{\rm ex}$ is the amplitude of the sinusoidal signal, which is to be optimized, f_i is the frequency of the injected signal, which is chosen to be 0.5 and 0.05 Hz according to the experimental results [37], i_c is a variable that changes with k, a time index with a different time interval. Since fuel economy

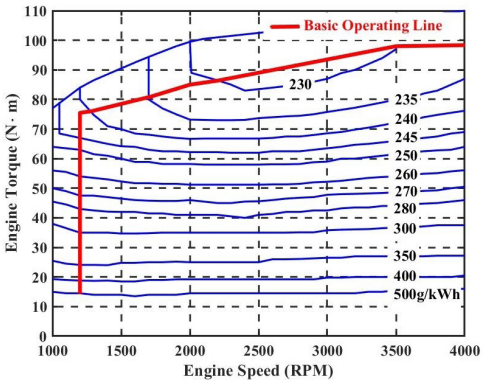

Fig. 5. Fuel consumption contours.

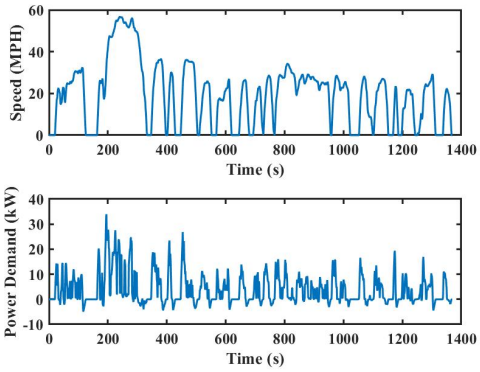

Fig. 6. Speed and power demand profile of the studied series HEV following UDDS.

optimization and battery parameter estimation are two conflicting objectives, the actively injected signal $I_{\text{ex}}\cos(2\pi f_i T_s j)$ without i_c will be compensated according to the simulation results. Therefore, the term, $i_c(k)$, which keeps constant in a time interval equal to half of the period of the injected signal, is added to the battery current in order to prevent the compensation. Since the period of i_c will be equal to or greater than the period of $I_{\text{ex}}\cos(2\pi f_i T_s j)$, the control of i_c cannot affect the injected signals. The formula of the battery power $P_b(j)$ can be linearly discretized from (6)

$$P_b(j) = V_0 i_b(j) - i_b^2(j) R_b. \tag{14}$$

The cost function $J_{\text{DP+}}$ for the DP with active signal injection, denoted as DP+, is then formulated as

$$J_{\text{DP+}} = \sum_{j=1}^{T_f} \phi(P_g(j) \times T_s) + \gamma\, \Delta_{\text{SOC}} \tag{15}$$

subject to the constraints

$$\begin{aligned} \text{SOC}_{\text{lb}} &\le \text{SOC}(j) \le \text{SOC}_{\text{ub}} \\ P_{g,\text{lb}} &\le P_g(j) \le P_{g,\text{ub}} \\ P_{(b,\text{lb})} &\le P_b(j) \le P_{b,\text{ub}} \\ i_{c,\text{lb}}(k) &\le i_c(k) \le i_{c,\text{ub}}(k) \\ \text{SOC}(T_f) &= \text{SOC}(1) \\ P_g(j) + P_b(j) &= P_d(j)/\eta_m(j) \end{aligned}$$

where $i_{c,\text{lb}}(k)$ and $i_{c,\text{ub}}(k)$, defined by (16), are the lower and upper bounds of the current variable i_c, respectively

$$\begin{cases} i_{c,\text{lb}}(k) = \max\limits_{T_p(k-1)\le T_s j \le T_p k} [i_{b,\text{lb}} - I_{\text{ex}}\cos(2\pi f_i T_s j)] \\ i_{c,\text{ub}}(k) = \min\limits_{T_p(k-1)\le T_s j \le T_p k} [i_{b,\text{ub}} - I_{\text{ex}}\cos(2\pi f_i T_s j)]. \end{cases} \tag{16}$$

T_p is the half period of the injected current signal, and $i_{b,\text{lb}}$ and $i_{b,\text{ub}}$ are the lower and upper bounds of the total battery current, respectively. T_s is set to be 0.2 and 1 s for the injected signals of 0.5 and 0.05 Hz, respectively.

With the new battery current signal obtained from DP+, the sequential algorithm discussed in Section III is applied and the detailed formulas are presented in the following.

Step 1: Due to the application of the high-pass filter and high-frequency current signal, the terminal voltage based on (11) can be simplified as

$$V_{\text{bf}}(s) = -R_e i_{\text{bf}}(s). \tag{17}$$

To estimate the ohmic resistance, i.e., R_e, the state-space equation of EKF is formulated as follows:

$$\begin{cases} \hat{R}_e(j) = \hat{R}_e(j-1) + r_j \\ V_{\text{bf}}(j) = -\hat{R}_e i_{\text{bf}}(j) + v_j \end{cases} \tag{18}$$

where r_j is defined as the process noise and v_j is defined as the measurement noise.

Step 2: After injecting the medium-frequency signal, (11) can be transformed into (19) because the ohmic resistance and RC pair dynamics will govern the filtered signal, i.e., V_{bf}

$$V_{\text{bf}}(s) = -R_e i_{\text{bf}}(s) - R_p i_{\text{bf}}(s)/(1+\tau_p s). \tag{19}$$

Using the estimated value of the ohmic resistance acquired in Step 1, the state-space equation of the EKF obtained from the bilinear transform is shown as follows:

$$\begin{cases} [\hat{R}_p(j)\ \hat{\tau_p}(j)]^T = [\hat{R}_p(j-1)\ \hat{\tau_p}(j-1)]]^T + r_j \\ V_{\text{bf}}(j) = -\hat{R}_e(j) i_{\text{bf}}(j) - \hat{R}_p i_2(j) + v_j \end{cases} \tag{20}$$

where

$$i_2(j) = \frac{T_s[i_{\text{bf}}(j) + i_{\text{bf}}(j-1)]}{T_s + 2\hat{\tau_p}} - \frac{T_s - 2\hat{\tau_p}}{T_s + 2\hat{\tau_p}} i_2(j-1).$$

Step 3: Applying the estimated ohmic resistance and parameters of the RC pair, the equation of SOC/SOH co-estimation obtained from linear discretization can be presented as follows:

$$\begin{cases} \hat{Q}_b(j) = \hat{Q}_b(j-1) + r_j \\ \mathbf{X}_3(j) = \begin{bmatrix} e^{-\frac{T_s}{\hat{\tau_p}}} & 0 \\ 0 & 1 \end{bmatrix} \mathbf{X}_3(j-1) + \mathbf{B} i_b(j) \\ V_b(j) = V_C(z(j)) - V_p(j) - \hat{R}_p(j) i_b(j) \end{cases} \tag{21}$$

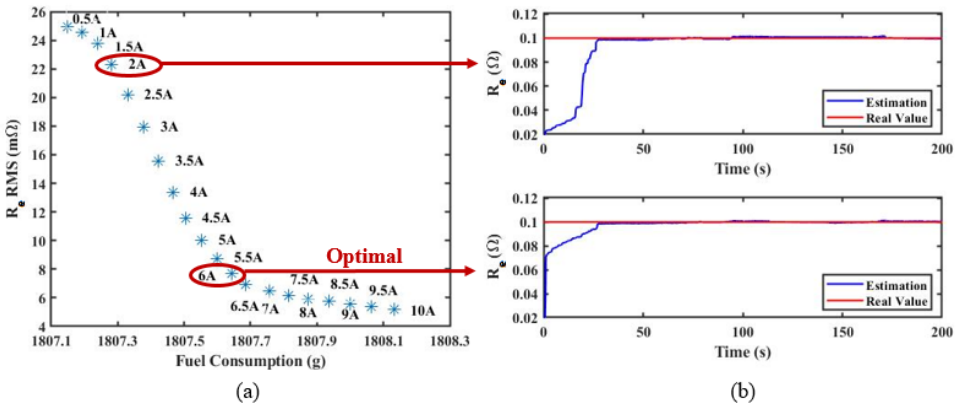

Fig. 7. (a) Tradeoff between estimation accuracy and fuel economy. (b) Comparison between estimation using different current signals.

where

$$\mathbf{X}_3(j) = \left[V_p(j)\ z(j)\right]^T$$

$$\mathbf{B} = \left[\hat{R}_p\left(1 - e^{-\frac{T_s}{\hat{\tau}_p}}\right)\ -\frac{\eta T s}{\hat{Q}_b}\right]^T.$$

The voltage of the RC pair (i.e., V_p) is identified in the sequential algorithm to improve the estimation accuracy [33].

V. Simulation Results

Simulations of the series HEV model are conducted using the Urban Dynamometer Driving Schedule (UDDS). According to its speed profile shown in Fig. 6 and (3)–(5), the power demand profile for the studied series HEV is obtained. Some basic information about UDDS is listed as follows: 1) the cycle time is 1370 s; 2) the maximum vehicle speed is 56.7 MPH; and 3) the driving distance is 7.45 mi.

A. Tradeoff Between Parameters' Estimation and Fuel Economy

Since a larger signal amplitude can improve estimation accuracy but increase fuel consumption, there is a tradeoff between these different objectives. To explore this relationship, the amplitude of the injected current signal (i.e., I_{ex}) is set to range from 0.5 to 10 A. Since the driving distance for one driving cycle is only 7.45 mi, the simulations are conducted over five consecutive cycles. According to experimental results [37], the effectiveness of the sequential algorithm is verified and it takes less than 200 s for the estimated ohmic resistance of the battery cell to converge. Therefore, the 0.5-Hz active signal is only injected for the first 200 s of the process to minimize the increase of fuel consumption, and the ohmic resistance is identified according to the results of DP+. The root mean square (rms) of the estimation error for the ohmic resistance is defined as

$$\text{rms Error} = \sqrt{\frac{\sum_{i=1}^{T}\left(\hat{R}_e - R_e\right)^2}{T}} \tag{22}$$

where T is the total time length. The rms error is used to indicate the identification accuracy. As shown in Fig. 7(a), the estimation accuracy can be improved by increasing I_{ex}, but the fuel consumption increases. However, the benefit of increasing I_{ex} is not significant when I_{ex} is beyond a transition area. The "knee point" can be defined when $I_{\text{ex}} = 6$ A, and this specific amplitude is chosen for the active signal injection in Section V-B. The estimation results when injecting current signals with different amplitudes (i.e. $I_{\text{ex}} = 2$ A or 6 A are also compared, as shown in Fig. 7(b). This reveals that the signal with a larger amplitude can provide richer information for parameters/states estimation because the estimated ohmic resistance converges to the actual value faster.

B. System Optimization

According to the power demand profile shown in Fig. 6, the baseline DP− is applied to solve the energy management problem. The penalty factor γ is chosen to be 350 in the simulation. According to Fig. 8(a), the total fuel consumption of the baseline DP− is 1795.13 g when no signal is injected. The fluctuation range of the battery SOC is narrow according to Fig. 8(a) because the studied HEV is not a plug-in hybrid system and so the battery capacity is small.

Then, a 0.5-Hz sinusoidal signal is injected for the first 200 s. According to Fig. 8(b), the total fuel consumption is 1807.64 g, an increase of 0.69% when compared to the result of DP−. The SOC profile, which is shown in Fig. 8(b), illustrates that the battery keeps being charged for the first 200 s, meaning that the ICE supplies power to both the vehicle, to follow the driving cycle, and the battery for actively injecting the signal. Compared with the simulation results of DP−, where the battery has to supply power at the very beginning, the results of DP+ show that the battery needs to be charged initially to ensure the injection of the active signal is successful. Specifically, the engine is turned on during idle periods (i.e., zero power demand) to provide the excitation signals with enough richness to the battery for the identification purpose. Furthermore, the battery SOC fluctuates in a wide range, meaning that the battery is effectively used.

Similarly, a sinusoidal signal with a frequency of 0.05 Hz is injected. The injection period is set to be 500 s according to the experimental results [37]. The results, shown in Fig. 8(c), illustrates that the fuel consumption for five driving cycles

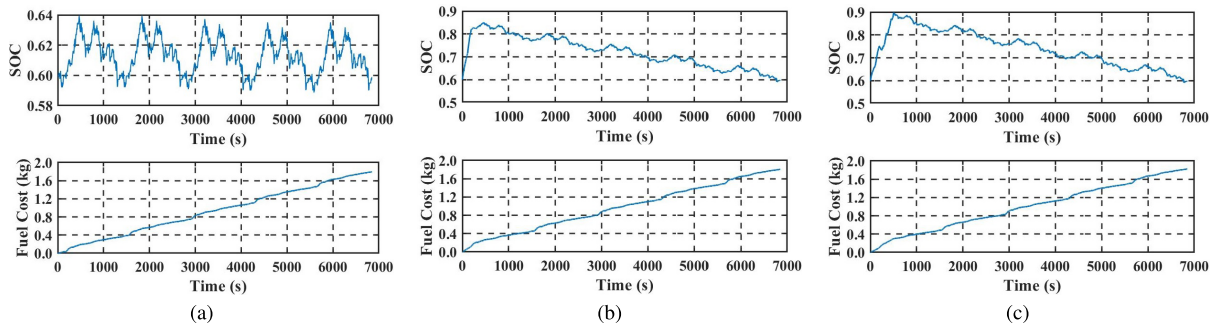

Fig. 8. Simulation results under different conditions. (a) DP−. (b) DP+ with 0.5-Hz signal. (c) DP+ with 0.05-Hz signal.

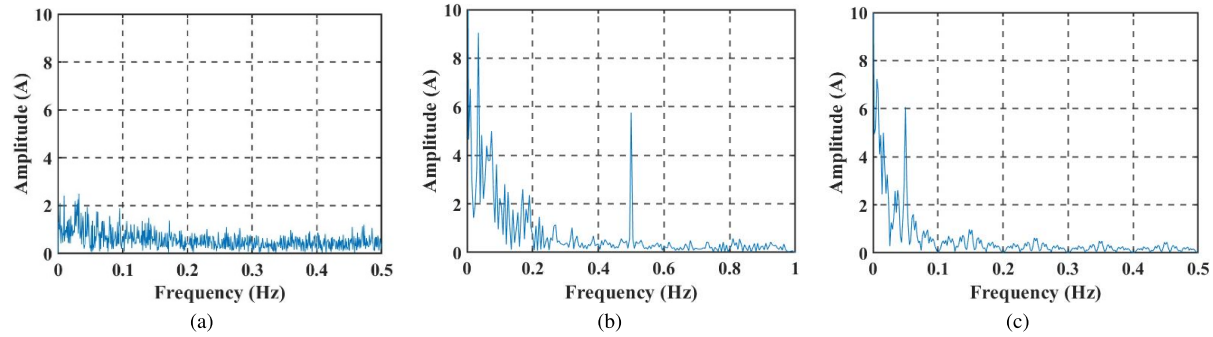

Fig. 9. Fast Fourier transform of battery current. (a) DP−. (b) DP+ with 0.5-Hz signal. (c) DP+ with 0.05-Hz signal.

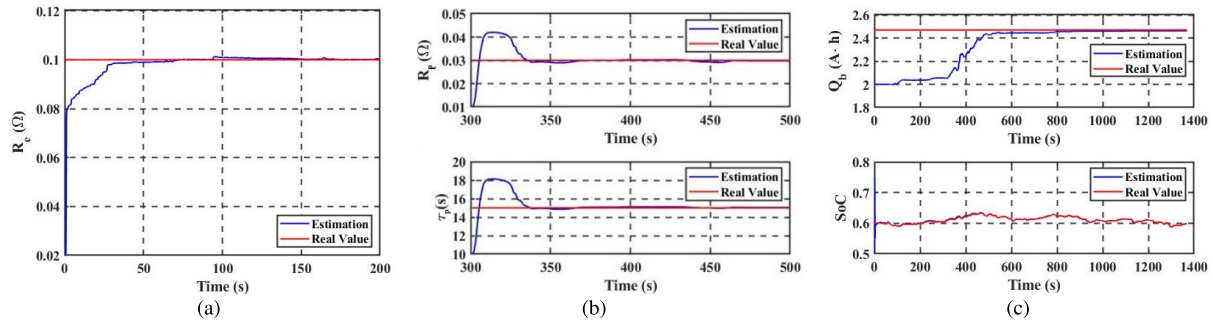

Fig. 10. Estimation results of DP+. (a) Ohmic resistance. (b) Parameters of RC pair. (c) Capacity and SOC.

is 1825.02 g, an increase of 1.67% when compared with the baseline DP−. As shown in Fig. 8(c), the SOC also fluctuates over a wide range, which increases the system efficiency after the injection of active signals is turned off. In addition, the current profiles for different cases are analyzed in the frequency domain. The maximum current amplitude is close to 2 A as shown in Fig. 9(a), which means that the richness of the baseline current signal is insufficient for estimation. The current fluctuations in Fig. 9(a) are caused by the vehicular dynamics under the studied driving cycle. Applying the proposed DP+, the current signals with the desired frequencies (i.e., 0.5 and 0.05 Hz) are injected successfully because their amplitudes increase to 6 A, according to Fig. 9(b) and (c). The additional current component, $i_c(k)$, introduces a low-frequency current with large amplitude because the time interval of k is larger than the period of the injected signals.

C. Battery Parameter/State Estimation

After the simulations using the proposed DP+, battery parameter/state identification is conducted using the acquired current profiles. The sequential algorithm, based on the first-order ECM, is adopted in the estimation process. In order to simulate real-life effects, white noise with an rms value of 10 mV is added to the voltage measurement. The identified parameters and states are initially chosen to be $[R_e(1)\ R_p(1)\ \tau_p(1)\ Q_b(1)\ \mathrm{SOC}(1)] = [0.02\ 0.01\ 10\ 2\ 0.5]$. In the first step of the sequential algorithm, a high-pass filter with 0.2-Hz cutoff frequency is chosen and EKF is used to identify the battery cell resistance. The estimated resistance is able to track the actual value quickly according to Fig. 10(a). In Step 2, a high-pass filter with 0.02-Hz cutoff frequency is selected. The estimation process starts at 300 s so that the initial SOC dynamics can be filtered. As shown in Fig. 10(b), the identified parameters (i.e., R_p and τ_p) can track the actual values accurately. In Step 3, SOH and SOC are estimated simultaneously based on the previously identified parameters. No excitation current needs to be injected in this step because the estimation of SOC is not affected by current frequency, while the identification of SOH prefers low current frequencies [37]. According to Fig. 10(c), the estimated

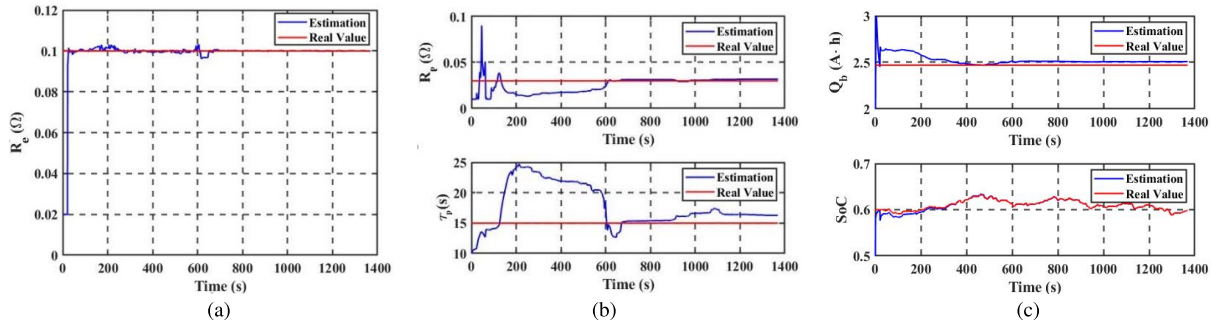

Fig. 11. Estimation results of DP-(parameters and states of battery are identified concurrently using DEKF). (a) Ohmic resistance. (b) Parameters of *RC* pair. (c) Capacity and SOC.

capacity and SOC converge to the actual values in just one driving cycle. Therefore, it is verified that the identification of states/parameters is accurate using the sequential algorithm.

For comparison, all the battery parameters/states are identified concurrently based on the multiscale DEKF using the current profile acquired from the baseline DP−. The initial conditions and noise are set to be the same as those applied in the sequential algorithm. According to Figs. 10(a) and 11(a), the rms error of the ohmic resistance estimation based on multiscale DEKF increases by 100% when compared to the simulation results using the proposed DP+ and the sequential algorithm. Although the identified R_e converges to the actual value, it takes a longer time (i.e., 700 s, which is more than three times the required time applying the sequential algorithm), thus, the rms error obtained from (22) increases from 1.1 to 5.9 mΩ. The time interval for the estimated R_p to track its actual value is 600 s, which is larger than the corresponding time interval using the sequential algorithm. In addition, the estimated τ_p and Q_b cannot track the actual values and there are significant static errors, as shown in Fig. 11(b) and (c).

VI. Conclusion

Based on the overactuated nature of the series HEV, SIC can be adopted in order to make sure that the battery is used in a safe and efficient manner. DP is used to optimize the fuel economy when active signals are injected for battery parameters/states estimation through the sequential algorithm. The method of how to successfully inject the signals is described (i.e., the battery current should have a constant value for every half period of excitation) and verified to be reasonable using the proposed DP. In addition, the tradeoff between fuel consumption and identification accuracy is exploited in order to provide a guideline for active signal injection (i.e., 6 A is chosen to be the amplitude of the sinusoidal component of the battery current for this specific case). According to the simulation results, injecting active signals can improve identification accuracy of battery parameters/states by more than 100% and the increase of fuel consumption is slight, only 0.69% and 1.67% for different steps of the sequential algorithm. In future work, the proposed combination of active signal injection and the sequential algorithm can be investigated in other power management scenarios using alternative control methods, such as model predictive control, for real-time implementation. In addition, the effectiveness of SIC can be studied for other configurations of HEVs, such as parallel HEVs and power-split HEVs.

References

[1] Z. Wei, J. Xu, and D. Halim, "HEV power management control strategy for urban driving," *Appl. Energy*, vol. 194, pp. 705–714, May 2017.

[2] J. Hou and Z. Song, "A hierarchical energy management strategy for hybrid energy storage via vehicle-to-cloud connectivity," *Appl. Energy*, vol. 257, Jan. 2020, Art. no. 113900.

[3] C. Yang, Y. Shi, L. Li, and X. Wang, "Efficient mode transition control for parallel hybrid electric vehicle with adaptive dual-loop control framework," *IEEE Trans. Veh. Technol.*, to be published.

[4] A. Santucci, A. Sorniotti, and C. Lekakou, "Power split strategies for hybrid energy storage systems for vehicular applications," *J. Power Sources*, vol. 258, pp. 395–407, Jul. 2014.

[5] D. Liu, Y. Song, L. Li, H. Liao, and Y. Peng, "On-line life cycle health assessment for lithium-ion battery in electric vehicles," *J. Cleaner Prod.*, vol. 199, pp. 1050–1065, Oct. 2018.

[6] H. Guo, X. Wang, and L. Li, "State-of-charge-constraint-based energy management strategy of plug-in hybrid electric vehicle with bus route," *Energy Convers. Manage.*, vol. 199, Nov. 2019, Art. no. 111972.

[7] A. Widodo, M.-C. Shim, W. Caesarendra, and B.-S. Yang, "Intelligent prognostics for battery health monitoring based on sample entropy," *Expert Syst. Appl.*, vol. 38, no. 9, pp. 11763–11769, Sep. 2011.

[8] A. M. Dizqah, B. Lenzo, A. Sorniotti, P. Gruber, S. Fallah, and J. De Smet, "A fast and parametric torque distribution strategy for four-wheel-drive energy-efficient electric vehicles," *IEEE Trans. Ind. Electron.*, vol. 63, no. 7, pp. 4367–4376, Jul. 2016.

[9] A. Hasanzadeh, D. M. Reed, and H. F. Hofmann, "Rotor resistance estimation for induction machines using carrier signal injection with minimized torque ripple," *IEEE Trans. Energy Convers.*, vol. 34, no. 2, pp. 942–951, Jun. 2019.

[10] D. M. Reed, J. Sun, and H. F. Hofmann, "Simultaneous identification and adaptive torque control of permanent magnet synchronous machines," *IEEE Trans. Control Syst. Technol.*, vol. 25, no. 4, pp. 1372–1383, Jul. 2017.

[11] Weiss, F. Leve, I. V. Kolmanovsky, and M. Jah, "Reaction wheel parameter identification and control through receding horizon-based null motion excitation," in *Advances in Estimation, Navigation, and Spacecraft Control*. Heidelberg, Germany: Springer, 2015, pp. 477–494.

[12] Y. Chen and J. Wang, "Fast and global optimal energy-efficient control allocation with applications to over-actuated electric ground vehicles," *IEEE Trans. Control Syst. Technol.*, vol. 20, no. 5, pp. 1202–1211, Sep. 2012.

[13] Z. Song *et al.*, "Simultaneous identification and control for hybrid energy storage system using model predictive control and active signal injection," *IEEE Trans. Ind. Electron.*, to be published.

[14] C. C. Chan, "The state of the art of electric, hybrid, and fuel cell vehicles," *Proc. IEEE*, vol. 95, no. 4, pp. 704–718, Apr. 2007.

[15] X. Wang, L. Li, and C. Yang, "Hierarchical control of dry clutch for engine-start process in a parallel hybrid electric vehicle," *IEEE Trans. Transport. Electrific.*, vol. 2, no. 2, pp. 231–243, Jun. 2016.

[16] Y. Huang, H. Wang, A. Khajepour, H. He, and J. Ji, "Model predictive control power management strategies for HEVs: A review," *J. Power Sources*, vol. 341, pp. 91–106, Feb. 2017.
[17] M. Sorrentino, G. Rizzo, and I. Arsie, "Analysis of a rule-based control strategy for on-board energy management of series hybrid vehicles," *Control Eng. Pract.*, vol. 19, no. 12, pp. 1433–1441, Dec. 2011.
[18] L. Li, X. Wang, and J. Song, "Fuel consumption optimization for smart hybrid electric vehicle during a car-following process," *Mech. Syst. Signal Process.*, vol. 87, pp. 17–29, Mar. 2017.
[19] S. G. Wirasingha and A. Emadi, "Classification and review of control strategies for plug-in hybrid electric vehicles," *IEEE Trans. Veh. Technol.*, vol. 60, no. 1, pp. 111–122, Jan. 2011.
[20] C. Yang, S. You, W. Wang, L. Li, and C. Xiang, "A stochastic predictive energy management strategy for plug-in hybrid electric vehicles based on fast rolling optimization," *IEEE Trans. Ind. Electron.*, to be published.
[21] L. Serrao, S. Onori, and G. Rizzoni, "A comparative analysis of energy management strategies for hybrid electric vehicles," *J. Dyn. Syst., Meas., Control*, vol. 133, no. 3, pp. 031012-1–031012-9, 2011.
[22] S. Feng, H. Sun, Y. Zhang, J. Zheng, H. X. Liu, and L. Li, "Tube-based discrete controller design for vehicle platoons subject to disturbances and saturation constraints," *IEEE Trans. Control Syst. Technol.*, to be published.
[23] Z. Wei, T. M. Lim, M. Skyllas-Kazacos, N. Wai, and K. J. Tseng, "Online state of charge and model parameter co-estimation based on a novel multi-timescale estimator for vanadium redox flow battery," *Appl. Energy*, vol. 172, pp. 169–179, Jun. 2016.
[24] X. Lin *et al.*, "A lumped-parameter electro-thermal model for cylindrical batteries," *J. Power Sources*, vol. 257, pp. 1–11, Jul. 2014.
[25] X. Hu, S. Li, and H. Peng, "A comparative study of equivalent circuit models for Li-ion batteries," *J. Power Sources*, vol. 198, pp. 359–367, Jan. 2012.
[26] G. Plett, "Extended Kalman filtering for battery management systems of LiPB-based HEV battery packs: Part 3. State and parameter estimation," *J. Power Sources*, vol. 134, no. 2, pp. 277–292, Aug. 2004.
[27] I.-S. Kim, "The novel state of charge estimation method for lithium battery using sliding mode observer," *J. Power Sources*, vol. 163, no. 1, pp. 584–590, Dec. 2006.
[28] Z. Wei, C. Zou, F. Leng, B. H. Soong, and K.-J. Tseng, "Online model identification and state-of-charge estimate for lithium-ion battery with a recursive total least squares-based observer," *IEEE Trans. Ind. Electron.*, vol. 65, no. 2, pp. 1336–1346, Feb. 2018.
[29] P. Rong and M. Pedram, "An analytical model for predicting the remaining battery capacity of lithium-ion batteries," *IEEE Trans. Very Large Scale Integr. (VLSI) Syst.*, vol. 14, no. 5, pp. 441–451, May 2006.
[30] M. H. Lipu *et al.*, "A review of state of health and remaining useful life estimation methods for lithium-ion battery in electric vehicles: Challenges and recommendations," *J. Cleaner Prod.*, vol. 205, pp. 115–133, Dec. 2018.
[31] H. Rahimi-Eichi, F. Baronti, and M.-Y. Chow, "Online adaptive parameter identification and state-of-charge coestimation for lithium-polymer battery cells," *IEEE Trans. Ind. Electron.*, vol. 61, no. 4, pp. 2053–2061, Apr. 2014.
[32] S. Dey, B. Ayalew, and P. Pisu, "Nonlinear robust observers for state-of-charge estimation of lithium-ion cells based on a reduced electrochemical model," *IEEE Trans. Control Syst. Technol.*, vol. 23, no. 5, pp. 1935–1942, Sep. 2015.
[33] R. Xiong, F. Sun, Z. Chen, and H. He, "A data-driven multi-scale extended Kalman filtering based parameter and state estimation approach of lithium-ion polymer battery in electric vehicles," *Appl. Energy*, vol. 113, pp. 463–476, Jan. 2014.
[34] E. Wan and A. Nelson, "Dual extended Kalman filter methods," in *Kalman Filtering and Neural Networks*. New York, NY, USA: Wiley, 2001, pp. 123–173.
[35] M. J. Rothenberger, D. J. Docimo, M. Ghanaatpishe, and H. K. Fathy, "Genetic optimization and experimental validation of a test cycle that maximizes parameter identifiability for a Li-ion equivalent-circuit battery model," *J. Energy Storage*, vol. 4, pp. 156–166, Dec. 2015.
[36] M. Rothenberger, J. Anstrom, S. Brennan, and H. Fathy, "Maximizing parameter identifiability of an equivalent-circuit battery model using optimal periodic input shaping," in *Proc. Dyn. Syst. Control Conf.*, 2014, pp. 1–10.
[37] Z. Song *et al.*, "The sequential algorithm for combined state of charge and state of health estimation of lithium-ion battery based on active current injection," *Energy*, vol. 193, Feb. 2020, Art. no. 116732.
[38] S. Wang, C. Fernandez, M. Chen, L. Wang, and J. Su, "A novel safety anticipation estimation method for the aerial lithium-ion battery pack based on the real-time detection and filtering," *J. Cleaner Prod.*, vol. 185, pp. 187–197, Jun. 2018.
[39] N. Murgovski, L. Johannesson, J. Hellgren, B. Egardt, and J. Sjöberg, "Convex optimization of charging infrastructure design and component sizing of a plug-in series HEV powertrain," *IFAC Proc. Volumes*, vol. 44, no. 1, pp. 13052–13057, Jan. 2011.
[40] R. H. Staunton, C. W. Ayers, L. D. Marlino, J. N. Chiasson, and T. A. Burress, "Evaluation of 2004 Toyota Prius hybrid electric drive system," U.S. Dept. Energy, Washington, DC, USA, Tech. Rep., May 2006.
[41] J. Liu and H. Peng, "Modeling and control of a power-split hybrid vehicle," *IEEE Trans. Control Syst. Technol.*, vol. 16, no. 6, pp. 1242–1251, Nov. 2008.
[42] Z. Song, X. Wu, X. Li, J. Sun, H. F. Hofmann, and J. Hou, "Current profile optimization for combined state of charge and state of health estimation of lithium ion battery based on Cramer–Rao bound analysis," *IEEE Trans. Power Electron.*, vol. 34, no. 7, pp. 7067–7078, Jul. 2019.
[43] P. Ioannou and J. Sun, *Robust Adaptive Control*, vol. 1. North Chelmsford, MA, USA: Courier Corporation, 2012.
[44] C. Weng, Y. Cui, J. Sun, and H. Peng, "On-board state of health monitoring of lithium-ion batteries using incremental capacity analysis with support vector regression," *J. Power Sources*, vol. 235, pp. 36–44, Aug. 2013.
[45] Z. Song, H. Wang, J. Hou, H. F. Hofmann, and J. Sun, "Combined state and parameter estimation of lithium-ion battery with active current injection," *IEEE Trans. Power Electron.*, vol. 35, no. 4, pp. 4439–4447, Apr. 2020.
[46] N. Samad, J. Siegel, and A. Stefanopoulou, "Parameterization and validation of a distributed coupled electro-thermal model for prismatic cells," in *Proc. Dyn. Syst. Control Conf.*, 2014, pp. 1–9.
[47] J. H. Lee and N. L. Ricker, "Extended Kalman filter based nonlinear model predictive control," *Ind. Eng. Chem. Res.*, vol. 33, no. 6, pp. 1530–1541, Jun. 1994.
[48] C. Hu, B. D. Youn, and J. Chung, "A multiscale framework with extended Kalman filter for lithium-ion battery SOC and capacity estimation," *Appl. Energy*, vol. 92, pp. 694–704, Apr. 2012.
[49] K. Muta, M. Yamazaki, and J. Tokieda, "Development of new-generation hybrid system THS II drastic improvement of power performance and fuel economy," SAE Tech. Paper 2004-01-0064, 2004.

Haojie Zhu (Student Member, IEEE) is currently pursuing the bachelor's degree in mechanical engineering with the University of Michigan, Ann Arbor, MI, USA.

His research interests include control and optimization for hybrid electric vehicles and intelligent transportation systems.

Ziyou Song (Member, IEEE) received the B.E. and Ph.D. degrees (Hons.) in automotive engineering from Tsinghua University, Beijing, China, in 2011 and 2016, respectively.

He was a Research Scientist with Tsinghua University from 2016 to 2017. He is currently a Post-Doctoral Research Fellow with the Department of Naval Architecture and Marine Engineering and the Department of Electrical Engineering and Computer Science, University of Michigan, Ann Arbor, MI, USA. He is the author or coauthor of more than 50 peer-reviewed publications, including more than 40 journal articles. His research interests lie in the areas of modeling, estimation, optimization, and control of energy storage for electrified vehicles and renewable systems.

Dr. Song received several paper awards, including the Applied Energy 2015–2016 Highly Cited Paper Award, the Applied Energy Award for Most Cited Energy Article from China, the NSK Outstanding Paper Award of Mechanical Engineering, and the 2013 IEEE VPPC Best Student Paper Award.

Jun Hou (Member, IEEE) received the M.S. degree in electrical engineering from Northeastern University, Shenyang, China, in 2011, and the Ph.D. degree from the University of Michigan, Ann Arbor, MI, USA, in 2017.

His current research interests include integration, modeling, control, and optimization of hybrid energy storage, power electronic converters, and electric propulsion systems.

Heath F. Hofmann (Senior Member, IEEE) received the Ph.D. degree in electrical engineering and computer science from the University of California at Berkeley, Berkeley, CA, USA, in 1998.

He is currently a Professor with the University of Michigan, Ann Arbor, MI, USA. He has authored approximately four dozen articles in refereed journals. He currently holds 14 patents. His research interests include power electronics, specializing in the design, simulation, and control of electromechanical systems, adaptive control techniques, energy harvesting, flywheel energy storage systems, electric and hybrid electric vehicles, and finite-element analysis.

Jing Sun (Fellow, IEEE) received the B.S. and M.S. degrees from the University of Science and Technology of China, Hefei, China, in 1982 and 1984, respectively, and the Ph.D. degree from the University of Southern California, Los Angeles, CA, USA, in 1989.

From 1989 to 1993, she was an Assistant Professor with the Electrical and Computer Engineering Department, Wayne State University, Detroit, MI, USA. She joined the Ford Research Laboratory, Dearborn, MI, USA, in 1993, where she was with the Powertrain Control Systems Department. After spending almost ten years in industry, she came back to academia and joined the Faculty of the College of Engineering, University of Michigan, Ann Arbor, MI, in 2003, where she is currently the Michael G. Parsons Professor and the Chair of the Department of Naval Architecture and Marine Engineering, with courtesy appointments as a Professor with the Department of Electrical Engineering and Computer Science and the Department of Mechanical Engineering. She has coauthored a textbook on robust adaptive control. She holds 39 U.S. patents. Her research interests include system and control theory and its applications to marine and automotive propulsion systems.

Dr. Sun was a recipient of the 2003 IEEE Control System Technology Award.